筑　波　大　学

博 士 （医 学） 学 位 論 文

E7090, a Novel Selective Inhibitor of Fibroblast Growth Factor Receptors, Displays Potent Antitumor Activity and Prolongs Survival in Preclinical Models

（新規 FGFRs 選択的阻害剤 E7090 の前臨床モデルにおける抗腫瘍作用および延命作用に関する検討）

２０１７

筑波大学大学院博士課程人間総合科学研究科

宮野　沙里

Table of contents

Literature Review

The fibroblast growth factor (FGF) signaling pathway comprises 18 ligands and 4 FGF receptor (FGFR) subtypes, FGFR1, -2, -3, and -4, which are receptor-type tyrosine kinases. Upon ligand binding, FGFRs activate an array of downstream signaling pathways, such as the mitogen activated protein kinase (MAPK) and the phosphoinositide-3-kinase (PI3K)/Akt pathways (Dieci et al., 2013; Turner and Grose, 2010).

In cancer, FGFRs with genetic abnormalities (gene fusion, mutation, or amplification) activate their signaling pathways, which contribute to proliferation, survival, and migration of cancer cells, tumor angiogenesis, and drug resistance (Turner and Grose, 2010). These abnormalities have been reported to be involved in cancer types including lung cancer (Cancer Genome Atlas Research, 2012; Liao et al., 2013; Thomas et al., 2014; Wu et al., 2013), breast cancer (Andre and Cortes, 2015; Wu et al., 2013), multiple myeloma (Dieci et al., 2013), endometrial cancer (Byron et al., 2012), gastric cancer (Matsumoto et al., 2012), glioblastoma (Singh et al., 2012), cholangiocarcinoma (Arai et al., 2014), and urothelial cancer (Network, 2014; Williams et al., 2013; Wu et al., 2013). Therefore, FGFRs are considered promising targets for cancer therapy, and FGFR inhibitors may serve as therapeutic agents.

The most clinically advanced FGFR inhibitors are multi-target kinase inhibitors such as ponatinib, nintedanib, dovitinib, and lucitanib. These inhibitors suppress multiple tyrosine kinases, but FGFRs are not inhibited as strongly as other kinases such as vascular endothelial growth factor receptors (VEGFRs), platelet-derived growth factor receptor (PDGFR), or ABL1 (Carter et al., 2015). Therefore, these inhibitors seem to be unlikely to achieve the required drug exposure for sufficient inhibition of the FGFR signaling pathway in tumors in a clinical setting.

Recently, the field of FGFR targeting has progressed exponentially, and several

FGFR-selective inhibitors, such as AZD4547 (Gavine et al., 2012), NVP-BGJ398 (Guagnano et al., 2011), and JNJ-42756493 (Tabernero et al., 2015), are in clinical trials, including some Phase 2 studies, targeting patients who have genetic alterations of *FGFRs* (Carter et al., 2015). Although these inhibitors produced partial responses in some cancer patients harboring *FGFR* gene abnormalities in Phase 1 studies, all of them are still under clinical development. Especially, the contribution of these inhibitors to prolongation of survival time remains to be clarified. Thus, there is a need to develop novel compounds that show potent FGFR inhibitory activity, suitable physicochemical property, pharmacokinetics profile, and the ability to prolong survival.

Research Purpose and Objectives

To provide a novel therapeutic option for cancer harboring FGFR abnormalities, a novel compound with potent and selective FGFRs inhibitor with suitable physicochemical property, pharmacokinetics profile, and the ability to prolong survival has been explored. Here, I report the preclinical pharmacological analyses of a novel selective FGFR inhibitor, E7090. It is an orally available tyrosine kinase inhibitor with a new type of binding kinetic profile to FGFR1. The analyses included target binding, antitumor activity in several subcutaneous human cancer cell line xenograft models, and survival benefit in a preclinical lung metastasis model. E7090 is currently being investigated in a Phase 1 study (NCT 02275910).

Methods

Compounds

E7090, E7090 succinate, AZD4547, ponatinib, and PD173074 were synthesized at

Eisai Co. Ltd., in accordance with a previously reported procedures (Li et al., 2012; Thompson et al., 2005) and are described in patent publications WO 2014129477 (US 20140235614), WO 2016027781, WO 2008075068, and WO 2007075869. For *in vitro* studies, all compounds were prepared as a 20 mmol/L stock solution in dimethyl sulfoxide (DMSO) and diluted in the relevant assay media. For *in vivo* studies, E7090 was formulated in a 3.5% (v/v) DMSO/6.5% (v/v) Tween 80/5% (w/v) glucose solution, and the administration volume (0.2 mL/10 g body weight) was calculated from the body weight before administration. E7090 succinate was dissolved in distilled water and the administration volume (0.1 mL/10 g body weight) was calculated from the body weight before administration.

Cell lines and reagents

Cell lines were obtained from the American Type Culture Collection (from 1993 to 2013), Deutsche Sammlung von Mikroorganismen und Zellkulturen GmbH (in 2009 and 2010), European Collection of Authenticated Cell Cultures (from 2008 to 2012), Immuno-Biological Laboratories Co., Ltd. (from 1990 to 2005), and Japanese Collection of Research Bioresources Cell Bank (in 2009 and in 2013). All cell lines were authenticated by the cell banks with short tandem repeat (STR) analysis from 2013 to 2016.

Antibodies against phospho-FGFR (Tyr653/654), FGFR1, phospho-FRS2α (Tyr436), phospho-ERK1/2 (Thr202/Tyr204), ERK1/2, phospho-AKT (Ser473), and AKT were obtained from Cell Signaling Technology. An antibody against FGFR2 was obtained from Santa Cruz Biotechnology. An antibody against β-actin was obtained from Sigma-Aldrich. Peroxidase-conjugated secondary antibodies were obtained from Cell Signaling Technology.

Cell-free kinase inhibition assay

Inhibitory activities of E7090 against 93 purified recombinant protein kinases (including tyrosine kinases and serine threonine kinases) were examined by using an Off-Chip Mobility Shift Assay from Carna Biosciences, Inc.. Briefly, a DMSO solution of E7090 was mixed with enzyme, substrate, ATP, and metals such as magnesium, calcium, or manganese under appropriate buffer conditions for each protein kinases. The readout value of the reaction control (complete reaction mixture) was set as 0% inhibition, and the readout value of the background (in the absence of enzyme) was set as 100% inhibition; the percent inhibition of each test solution was then calculated. IC_{50} values (the half maximal inhibitory concentration) were calculated from plots of concentration versus percent inhibition by using Microsoft Excel or GraphPad Prism.

Kinetic interaction analysis against FGFR1

Experiments to determine the binding affinities and kinetic rate constants of interactions between compounds and FGFR1 were performed as described previously(Neumann et al., 2009; Neumann et al., 2011). Briefly, FGFR1 (final concentration 6.7 nmol/L) was preincubated with the reporter probe at a concentration equal to its binding affinity (Kd) in a reaction buffer consisting of 20 mmol/L 3-Morpholinopropanesulfonic acid (MOPS) (pH 7.0), 1 mM Dithiothreitol (DTT), and 0.01% Tween20. The final reaction volume was 10 µl in black NBS 384-well polypropylene plates. After transfer of serially diluted compounds, probe displacement was monitored for 60 min. Kd values were calculated by using the Cheng-Prusoff equation from the IC_{50} values obtained from the percentage displacement values at the last time point measured. Association rate constants of the inhibitors were calculated from the decay rate of probe displacement. Dissociation rate constants were determined as the product of Kd × association rate constant.

Cell proliferation assay

Cells (500 to 5000) were seeded in a 96-well cell culture plate in RPMI-1640 (WAKO) containing 10% (v/v) fetal bovine serum (FBS) (Sigma-Aldrich). One day after cell seeding, various concentrations of compounds were added, and the cells were incubated at 37°C for 3 to 14 days. Then Cell Counting Kit-8 (Dojindo Laboratories) was added to each well, followed by incubation for the appropriate time. The optical density (OD) of each well was measured at 450 nm (reference wavelength: 650 nm) with a SpectraMax 250 (Molecular Devices) or EnVision (Perkin Elmer) microplate reader.

In vitro signal inhibition analysis

SNU-16 cells were treated with the indicated concentrations of E7090 succinate in RPMI-1640 containing 10% FBS for 4 h and lysed with RIPA buffer (Sigma-Aldrich) containing protease and phosphatase inhibitors. The protein expression of the indicated proteins was detected by Western blot. The blots were developed with ECL Prime Western Blotting detection reagents (GE Healthcare), and chemiluminescence was detected with an Image Analyzer LAS-4000 (Fuji Film). The chemiluminescence intensity of each band was measured using Multi Gauge software (version 3.1, Fuji Film).

The percentage of phosphorylation was determined by the following formula:

$$\text{p-FGFRs (\% of control)} = 100 \times (T - Bt)/(C - Bc)$$

where

T is the chemiluminescence intensity of p-FGFRs in the drug-treated sample lane,

Bt is the chemiluminescence intensity of background in the drug-treated sample lane,

C is the chemiluminescence intensity of p-FGFRs in the control sample lane, and

Bc is the chemiluminescence intensity of background in the control sample lane.

Knockdown experiments

Small interfering RNAs (siRNAs) targeting mouse *Fgfr1* (FGFR1 Stealth Select RNA interference [RNAi] MSS204294), mouse *Fgfr2* (FGFR2 Stealth Select RNAi MSS204298), mouse *Fgfr3* (FGFR3 Stealth Select RNAi MSS204301) and mouse *Fgfr4* (FGFR4 Stealth Select RNAi MSS236498), Stealth RNAi Negative Control med GC (as a control for siFGFR1, -2, -3) and Stealth RNAi Negative Control low GC (as a control for siFGFR4) were purchased from Thermo Scientific. Transfection complexes were prepared in antibiotic-free and serum-free medium by mixing 1 μM of siRNA solution (final concentration 3 nM) and DharmaFECT4 tranfection reagents (Thermo Scientific, final concentration 0.1 μL/well) in accordance with the manufacturer's recommended protocol. Then 4T1 cells (500 cells/well) were incubated with transfection complexes for 72 h, and the effect of cell growth was detected using Cell-Counting Kit-8. The optical density (OD) of each well was measured at 450 nm (reference wavelength: 650 nm) with EnVision™ (Perkin Elmer) microplate reader. The differences in OD450nm-OD650nm between the Negative control-treated and si*Fgfr1-4* groups were analyzed by one-way analysis of variance followed by the Dunnett multiple comparison test (more than 3 groups; the Negative control vs si*Fgfr1*, si*Fgfr2* and si*Fgfr3*) or t-test (2 groups; the Negative control vs si*Fgfr4*). A value of $P < 0.05$ (2 sided) was considered statistically significant. Statistical analyses were performed using GraphPad Prism.

Mouse subcutaneous xenograft model

Mice were maintained under specific-pathogen-free conditions and housed in barrier facilities on a 12 h light/dark cycle, with food and water ad libitum. Animal experiments were conducted in accordance with the Institutional Animal Care and Use Committee guidelines of Eisai Co., Ltd.

Cultured human cancer cells were prepared in Hank's Balanced Salt Solution

(Thermo Fisher Scientific Inc.) and mixed with an equal volume of BD Matrigel (BD Bioscience) to yield a suspension of 3.6×10^7 to 9.0×10^7 cells/mL. A 0.1 mL aliquot of the cell suspension was transplanted subcutaneously into the right flank region of female nude mice (7 weeks old, CLEA Japan or Japan SLC). When tumor volumes reached around 100–300 mm^3, mice were selected based on their tumor volumes and general condition, and were randomly divided into groups according to their tumor volumes (n = 4–6 per group). The oral administration of E7090 or E7090 succinate (6.25, 12.5, 25, or 50 mg/kg) or vehicle (control) was started on day 1, and the administration continued once daily for 11 to 14 days. The tumor was measured in two dimensions, and the volume was calculated using the following formula: tumor volume (mm^3) = 1⁄2 length (mm) × [width (mm)]^2.

The differences in tumor volume between the vehicle-treated and E7090 or E7090 succinate–treated groups were analyzed by one-way analysis of variance followed by the Dunnett multiple comparison test. A value of $P < 0.05$ (2 sided) was considered statistically significant. Statistical analyses were performed using GraphPad Prism.

SNU-16 tumors and plasma samples were collected at the indicated times after single oral administration. Nude mice bearing SNU-16 tumors were prepared as described above. Mice were given vehicle (n = 5) or indicated doses of E7090 (n = 3 per group) orally, and blood samples and tumors were collected at the indicated times.

Plasma concentrations of E7090 were determined by liquid chromatography-tandem mass spectrometry (LC-MS/MS). In short, plasma samples and standards were deproteinized with methanol-acetonitrile (3:7 [v/v]) containing an internal standard and centrifuged. The supernatant was then filtered and analyzed by LC-MS/MS.

For signal inhibition analysis, tumors were homogenized and lysed with Cell Lysis Buffer (Cell Signaling Technology) containing protease and phosphatase inhibitors. The protein expression of the indicated proteins was detected and the band intensity was

measured as described above. The ratio of phosphorylated FGFRs to total FGFR2 was calculated for each sample. Then the percentage of phosphorylation was determined by the following formula:

p-FGFRs/FGFR2 (% of control) = 100 × T'/C'

where

T' is the ratio of p-FGFRs/FGFR2 for the drug-treated sample lane, and

C' is the ratio of p-FGFRs/FGFR2 for the control sample lane.

Plasma FGF23 measurement

Nude mice bearing SNU-16 tumors were prepared as described above and administered vehicle (n = 5) or the indicated doses of E7090 (n = 3 per group) orally. Twenty-four hours later, plasma was collected, and the amount of plasma FGF23 was measured by using an FGF23 ELISA kit (Kainos Laboratories) in accordance with the manufacturer's procedure.

The differences in the amount of FGF23 between the vehicle-treated and E7090–treated groups were analyzed by one-way analysis of variance followed by the Dunnett multiple comparison test. A value of $P < 0.05$ (2 sided) was considered statistically significant. Statistical analyses were performed using GraphPad Prism.

4T1 lung metastasis model

The 4T1 lung metastasis mouse model was established as previously reported (Dey et al., 2010) with some modification. Briefly, 5×10^4 4T1 cells were injected into the tail veins of female Balb/c mice (8 weeks old, Charles River Japan). Eleven days after the cell injection, the mice were randomly divided into groups (n = 8 per group) and treated with vehicle or various concentrations of E7090 (orally, once daily). Mice were sacrificed according to the guideline for animal experiment of Eisai Co., Ltd.

Survival times between the E7090-treated group and the vehicle-treated group were compared with the log-rank (Mantel-Cox) test. Values of $P < 0.01$ were considered statistically significant. Statistical analyses were performed using GraphPad Prism.

Results

E7090 shows selective inhibition of FGFR tyrosine kinases 1-3

E7090, 5-({2-[({4-[1-(2-Hydroxyethyl)piperidin-4-yl]phenyl}carbonyl)amino]pyridin-4-yl}oxy)-6-(2-methoxyethoxy)-*N*-methyl-1*H*-indole-1-carboxamide, was synthesized as an orally available and selective inhibitor of FGFR1, -2, and -3. The structure of E7090 succinate is shown in Figure 1A. In this research, either E7090 or E7090 succinate was used in each study. To evaluate the selectivity of E7090 against FGFR1, -2, and -3, a kinase inhibition assay against 93 kinases, including wild-type and mutated members of the FGFR family, other receptor tyrosine kinases, and serine/threonine kinases was performed (Figure 1B and Supplementary Table S1). The IC_{50} values of E7090 on the enzymatic activity of FGFR1, -2, -3, and -4 were 0.71, 0.50, 1.2, and 120 nmol/L, respectively. The IC_{50} values of E7090 against mutated forms of FGFR3 (K650E and K650M) were 3.1 and 16 nmol/L, respectively. In addition, E7090 inhibited only 3 additional tyrosine kinases (RET, DDR2, and FLT1) with IC_{50} values lower than 10 nmol/L among the 93 kinases. A kinome map is shown in Supplementary Figure S1. These results indicate that E7090 is a selective inhibitor against FGFR1, -2, and -3 tyrosine kinases.

The interaction of E7090 with FGFR1 kinase possesses unique kinetics

To gain insight into the mode of interaction between E7090 succinate and FGFR1, the kinetics of the interaction was analyzed by using the Proteros reporter displacement

assay (Okamoto et al., 2015). The kinetic parameters for the interactions of FGFR1 with AZD4547 and ponatinib, which, from their co-crystal structures, are representative type I and type II FGFR1 inhibitors, respectively (Tucker et al., 2014) were also determined. The k_{on} and k_{off} values of E7090 succinate were 3.4×10^5 s^{-1} M^{-1} and 8.6×10^{-4} s^{-1}, resulting in a Kd value of 2.5 nmol/L (Table 1). The kinetic parameters for the interactions of AZD4547 and ponatinib with FGFR1 were consistent with the reported features of the interaction modes of these inhibitors (Tucker et al., 2014). Ponatinib had relatively slow association and dissociation kinetics, with a residence time of 57 min. In contrast, AZD4547 had fast association and dissociation kinetics, with a residence time of 7 min. E7090 succinate had interaction kinetics with FGFR1 kinases intermediate between those of the two representative inhibitors, and the residence time of E7090 succinate was 19 min. These data suggest that the interaction of E7090 with FGFR1 possesses unique kinetics among selective FGFR inhibitors, similar to that of type V inhibitors (Okamoto et al., 2015).

E7090 inhibits phosphorylation of FGFR and cell proliferation of SNU-16 cells

To evaluate the inhibitory activity of E7090 on the cellular FGFR signaling pathway, SNU-16 cells were treated with the indicated concentrations of E7090 succinate, and cell lysates were prepared for Western blotting analysis. SNU-16 is a human gastric cancer cell line which contains high copy numbers of *FGFR2* and high levels of FGFR2 protein expression and tyrosine phosphorylation (Kunii et al., 2008; Xie et al., 2013). E7090 succinate inhibited FGFR phosphorylation with an IC_{50} value of 1.2 nmol/L (Figure 2). E7090 treatment also inhibited the phosphorylation of FRS2α, ERK1/2, and AKT, molecules downstream of FGFRs, in a dose-dependent manner (Supplementary Figure S2). E7090 succinate inhibited SNU-16 cell proliferation with an IC_{50} value of 5.7 nmol/L

(Figure 3A), in a good agreement with the *in vitro* inhibition of FGFR phosphorylation.

E7090 has selective anti-proliferative activity against cancer cell lines harboring *FGFR* abnormalities

E7090 was tested on a panel of 39 human cancer cell lines in cell proliferation assays (Supplementary Table S2). The IC_{50} values observed ranged from 2 nmol/L to greater than 10,000 nmol/L (Figure 3B). Thirteen cell lines were highly sensitive to E7090, with IC_{50} values less than 100 nmol/L. In this group of cell lines, 12 of the 13 cell lines harbored an *FGFR* abnormality, including *FGFR1* and/or *FGFR2* amplification, *FGFR1* fusion, *FGFR2* mutation, *FGFR3* mutation, or *FGFR3* fusion. These data indicate that E7090 has selective anti-proliferative activity against cancer cell lines harboring *FGFR* genetic abnormalities.

E7090 has antitumor activity and inhibits FGFR signaling in a mouse xenograft model of SNU-16 human gastric cancer

Next, the *in vivo* characteristics of E7090 were investigated in a SNU-16 subcutaneous xenograft model. Nude mice bearing SNU-16 xenografts were orally treated with various concentrations of E7090 succinate once daily for 14 days. Administration of 6.25 to 50 mg/kg E7090 succinate significantly inhibited tumor growth (Figure 4A) without severe loss of body weight (Figure 4B). To confirm the selective antitumor activity of E7090 against tumors harboring *FGFR* gene abnormalities *in vivo*, additional *in vivo* experiments using several human cancer cell lines were performed (Table 2). E7090 also had dose-dependent antitumor activity against other xenograft tumors harboring *FGFR* abnormalities such as *FGFRs* amplifications or fusions (NCI-H1581, DMS114, RT112/84 or MFM223), whereas even a dose of 50 mg/kg E7090 lacked

antitumor activity against xenograft tumors with no *FGFR* abnormalities (MCF-7, HCC1806, HCC1427, or MDA-MB-468). These data indicate that E7090 has selective anti-tumor activity against xenograft tumors harboring *FGFR* genetic abnormalities such as amplifications or fusions.

Next, a pharmacodynamic analysis of the level of FGFR phosphorylation in tumors in nude mice bearing SNU-16 tumors was performed. FGFR phosphorylation was inhibited by E7090 in a dose-dependent and time-dependent manner as assessed in a Western blotting analysis. E7090 at doses of 6.25 to 50 mg/kg reduced phosphorylation of FGFR to less than 10% of control levels at 4 h after oral administration (Figure 5A and Supplementary Figure S3), after which the level of FGFR phosphorylation recovered to the control level by 24 h. In the 50 mg/kg dosing group, maximal inhibition of FGFR phosphorylation lasted for 12 h after drug administration. The effect of E7090 on plasma FGF23 level was also examined. FGF23 belongs to a subgroup of FGF ligands that function as endocrine factors, and elevation of plasma FGF23 has been demonstrated to be a surrogate pharmacodynamic biomarker of FGFR inhibition in both nonclinical and clinical studies (Kim et al., 2011; Wohrle et al., 2011). Dose-dependent elevation of plasma FGF23 was observed at 24 h after drug administration (Figure 5B).

In addition, a pharmacokinetic analysis of E7090 in nude mice bearing SNU-16 tumors was conducted. E7090 showed dose-dependent increase of maximum concentration (Cmax) and area under the curve (AUC) (Cmax values of 9.31, 23.8, 94.2, 179.7, and 415 ng/mL and AUC values of 27.5, 84.4, 228.5, 481.6 and 1172.6 ng · h/mL for 3.13, 6.25, 12.5, 25, and 50 mg/kg, respectively; Figure 5C).

E7090 treatment prolongs survival in a 4T1 mouse lung metastasis model

To evaluate the effect of E7090 on survival, we established a lung metastasis model using 4T1, a mouse breast cancer cell line, in Balb/c mice as a clinically relevant model.

E7090 inhibited tumor growth of 4T1 with an IC_{50} value of 22 nmol/L *in vitro* (Figure 6A). A siRNA knockdown experiment revealed that each *Fgfr2* siRNA or *Fgfr3* siRNA decreased cell growth of 4T1 cell, meaning that 4T1 cell growth is dependent on both FGFR2 and the FGFR3 signaling pathway (Supplementary Figure S4). The dependency of 4T1 cell growth on the FGFR signaling pathway was also confirmed by performing a cell proliferation assay using PD173074 (Figure 6A), another FGFR1, -2, and -3 inhibitor that has previously shown selective inhibitory activity against FGFR kinase in preclinical experiments (Mohammadi et al., 1998). Next, a challenge experiment was performed (Figure 6B). Cultured 4T1 cells were intravenously injected into mice, and 11 days after cell inoculation, engraftment of 4T1 cells was observed in the lung. On the day engraftment was observed, administration of E7090 was started. In this model, mice became moribund within 20 days, suffering from cancer-induced cachexia and pulmonary dysfunction. Daily administration of E7090 significantly prolonged the survival of mice in the 12.5 to 50 mg/kg dosing groups (Figure 6C and Table 3).

Discussion

We have developed E7090, an orally available selective inhibitor of the FGFR1, -2, and -3 tyrosine kinases with a unique kinetic profile among FGFR inhibitors. E7090 inhibited SNU-16 cell proliferation as expected from its *in vitro* inhibition of FGFR phosphorylation. E7090 shows selective anti-proliferative activity against cancer cell lines harboring *FGFR* abnormalities and showed antitumor activity in mouse subcutaneous xenograft models using cell lines with dysregulated FGFR signaling. Furthermore, E7090 administration significantly prolonged the lives of mice with lung metastases. Thus, E7090 is a selective FGFR inhibitor that shows promising antitumor activities with wide therapeutic windows in preclinical models of cancers harboring *FGFR* abnormalities.

Some multi-kinase inhibitors, including several FGFR-selective inhibitors and subtype-specific inhibitors, have been developed and are in clinical studies. Although some cancer patients harboring *FGFR* abnormalities have had partial responses in these clinical studies, none of them have exhibited any defined proof of concept in clinical studies. I present the first evidence that the interaction of E7090 with FGFR1 has unique kinetics that is different from those of other selective FGFR inhibitors. More than 80% of approved kinase inhibitors possess the characteristics of either type I inhibitors or type II inhibitors (Wu et al., 2016). Selective FGFR inhibitors such as AZD4547 have been reported to possess the characteristics of type I inhibitors. Generally, type I inhibitors have more rapid association and dissociation kinetics, whereas type II inhibitors such as ponatinib have slow binding kinetics, leading to a prolonged residence time (Liu and Gray, 2006; Tummino and Copeland, 2008). E7090 succinate associated more rapidly with FGFR1 than did ponatinib and E7090 dissociated more slowly and had a relatively longer resident time, than did AZD4547, which is a representative type I inhibitor. Our analysis revealed that E7090 possesses kinetic properties more similar to 4the type V inhibitors, such as lenvatinib, a VEGFR and multiple receptor tyrosine kinase inhibitor, which is the only type V kinase inhibitor approved for clinical use at this time (Wu et al., 2016). Further studies, including crystallization and co-structural determination of the FGFR1–E7090 complexes, are required to fully understand the details of E7090 binding to FGFRs at the amino acid level. In addition, the relationship between the unique binding kinetics of E7090 and its efficacy should be explored. For instance, mutations in the gatekeeper residues in kinase domain, which was known to cause the activation of tyrosine kinases, such as T790M in EGFR and T315I mutation in BCR-ABL were reported to induce conformational change of these protein structures and resistance against EGFR inhibitors erlotinib and gefitinib, and BCR-ABL inhibitor imatinib, respectively(Branford et al., 2002; Sutto and Gervasio, 2013; Yun et al., 2008;

Zhou et al., 2007). Similarly, mutation of the gatekeeper residue V561M in FGFR1 has been shown to confer *in vitro* drug resistance to FGFR inhibitors (Chell et al., 2013; Sohl et al., 2015). In addition, each N550H/K/S/T, E566A/G and K642N mutation in FGFR2 kinase domain is reported to induce dovitinib-resistance. These amino acid residues are part of a triad that forms a network of autoinhibitory hydrogen bonds termed the molecular brake and these mutations disrupt this molecular brake in the kinase hinge region of FGFR2(Byron et al., 2013). FGFR2 mutants at N550 and K642 have been reported in adenoid cystic carcinoma, breast cancer, endometrial cancer, head and neck cancer, gallbladder cancer, and spermatocytic seminoma(Gallo et al., 2015). From these reports, it is also hypothesized that differences of binding kinetics among FGFR inhibitors may affect inhibitory activity of each compounds against mutated type of FGFRs. In this article, I could not fully determine the inhibitory activity of E7090 against mutated type of FGFRs which have been reported in various cancers. Now, evaluation of inhibitory activity of E7090 against mutated type of FGFRs is on-going by using several transformants which have representative FGFR mutation and human cancer cell lines harboring FGFR mutations.

E7090 had selective anti-proliferative activity against cancer cell lines harboring *FGFR* abnormalities, but not all cell lines with these abnormalities were sensitive to E7090. One of the reasons is the protein expression level of FGFRs. In fact, some lung and breast cancer cell lines reported to have high copy numbers of *FGFR1*(Dutt et al., 2011; Turner et al., 2010; Weiss et al., 2010) were not sensitive to E7090, and I confirmed by Western blotting analysis that these cell lines in fact expressed low levels of FGFR1 (Supplementary Figure S5 and data not shown) (Kotani et al., 2016). Consistent with our results, J82, a human bladder cancer cell line harboring an FGFR3 K652E mutation, has been reported to be insensitive to FGFR inhibitors due to low protein expression (Lamont et al., 2011). Another reason may be activation of other signaling pathways,

which reduce activity of the FGFR inhibitor. Amplification of *PDGFRA* was also found in NCI-H1703 (Ramos et al., 2009). *KRAS* and RTK alterations occurred in a near mutually exclusive pattern, but *PIK3CA*, *PTEN* alterations, and *FGFR* alterations overlapped in patients with lung squamous carcinoma (Cancer Genome Atlas Research, 2012) and endometrial cancer (Byron et al., 2012). In squamous cell lung cancer, MYC was co-expressed in about 40% of *FGFR1*-amplified tumors, and this co-expression was associated with sensitivity to FGFR inhibitors (Malchers et al., 2014). These results suggest that in addition to the presence of *FGFR* abnormalities, the expression level of FGFRs or the status of other molecules should be investigated to select patients suitable for treatment with E7090.

E7090 showed antitumor activity in SNU-16 subcutaneous xenograft models in a dose-dependent manner without inducing severe weight loss. The Cmax value at a dose of 50 mg/kg, which is maximum tolerated dose (MTD) of E7090 in mice, is 415 ng/mL. The unbound Cmax value is calculated to be 12.5 ng/mL with unbound fraction in plasma (fu, 0.03), which is equivalent to 21.2 nmol/L. This result supports that there were few off-target effects even at the Cmax of the MTD dose. I also confirmed the mRNA expression level of *FGFR2* was more than 500-fold higher than those of *FLT-1*, *RET*, *DDR2*, *FLT-4*, *PDGFRA* and *KDR*, which E7090 showed inhibitory activity with IC_{50} values of lower than 20 nmol/L in cell-free kinase assay, in SNU-16 cells by using data extracted from the Cancer Cell Line Encyclopedia (CCLE) database (Barretina et al., 2012) (Data not shown). Combined with these data, I propose that antitumor activity of E7090 in SNU-16 sc xenograft model is based on inhibition of FGFR signaling and the possibility that inhibition of other targets involved in its activity in this model is low. Administration of E7090 produced dose-dependent increases of Cmax and AUC and sustained inhibition of FGFR phosphorylation in SNU-16 tumors, suggesting that the level of phosphorylated FGFRs would be an appropriate pharmacodynamic marker of

target inhibition by E7090. In addition, E7090 administration also elevated plasma FGF23 levels in a dose-dependent manner 24 h after administration, suggesting that plasma FGF23 is a good candidate biomarker for non-invasive estimation of target inhibition in humans. The dose dependent inhibition of tumor growth, FGFR phosphorylation and FGF23 elevation were consistent with the plasma exposure. Yamazaki et al., reported an excellent example of Pharmacokinetic/Pharmacodynamic (PK/PD) modeling using crizotinib, an orally available, ATP-competitive dual inhibitor for ALK and MET. They characterized the PK/PD relationships among crizotinib systemic concentration, ALK or MET inhibition, and tumor growth inhibition in human tumor xenograft models in a quantitative manner and have produced clinically applicable results (Yamazaki et al., 2012). Therefore, PK/PD modeling would be thought to be a useful approach linking drug exposure to pharmacologic responses as a function of time, providing a quantitative assessment of *in vivo* drug potency with mechanistic insight of drug action. We will investigate the relationship between the pharmacokinetic data and pharmacodynamic changes observed in the current study, such as phosphorylation of FGFR in tumors and increased plasma FGF23 levels, in preclinical models as a method to predict human dosing in near future.

In the setting of a clinical study, the survival benefit to patients is one of the most important endpoints for a new cancer therapeutic agent. Here, a mouse lung metastasis model was used to evaluate the effect of E7090 on survival. E7090 significantly prolonged the lives of mice in a dose-dependent manner. In this model, drug administration was started when 4T1 tumors grew in the lung 11 days after tumor cells were injected into the tail veins. This means that E7090 could be effective for metastases as well as primary lesions. However, even in the 50 mg/kg dosing group the mice became moribund and were euthanized. Further analysis of the residual tumors in the lung may help us to understand the mechanism of resistance and allow us to explore suitable drugs for use

in combination with E7090.

In this article, I mainly focused on antitumor activity of E7090 against cancer cells harboring FGFR gene abnormality. In addition to FGFRs gene alteration, FGF-FGFR autocrine/paracrine signaling in tumors is also known to be important in various cancer malignancy such as migration/invasion and metastasis. FGF-2 was reported to cause sustained activation of the MAPK-ERK pathway, leading to MMP-9 gene transcription and cellular invasion in the presence of N-cadherin and cancer cells acquire metastatic properties in breast cancer cells(Suyama et al., 2002). In regard with anti-metastatic activity, 4T1 lung metastasis model used in Figure 6B&C can't reflect process of cancer metastasis because tumor formation at lung has been completed at the timing of drug administration. To confirm the inhibitory activity of E7090 against metastasis, using other models, like 4T1 fat pad injection model or percutaneous injection model (Bailey-Downs et al., 2014; Rashid et al., 2014) should be needed.

To maximize antitumor effect of compounds, it is important to pay attention not only cancer cells but tumor microenvironment components such as and stromal/immune cells. In tumor microenvironment, several cancer cells release pro-fibrotic FGFs that act on cancer-associated fibroblasts (CAFs) and induce their activation; in turn, CAF-produced FGFs actively sustain growth and invasion of FGFRs-expressed tumors (Procopio et al., 2015). FGF2 is also reported to have a key role in wound healing and angiogenesis by promoting proliferation and migration of endothelial cells in murine models, particularly in combination with vascular endothelial growth factor (VEGF) (Ichikawa K and et al., 2016; WERNER and GROSE, 2003). In this article, the effect of E7090 against tumor microenvironment such as tumor vasculature or stroma cells etc. has not been clarified. Therefore, to find out the efficacy of E7090 as the modulator of tumor microenvironment, additional exploratory experiments are required.

In summary, I propose that E7090 could be a novel therapeutic agent for cancer

patients with abnormalities in the FGF/FGFR signaling pathway. Based on the preclinical results reported here, E7090 is currently being investigated in a Phase 1 clinical trial (NCT 02275910).

Conclusion

From these results, E7090 is clarified as a potent and selective FGFR1, 2 and 3 inhibitor showing antitumor activities in preclinical cancer models harboring FGFRs gene abnormalities and prolongation of survival in mice model. E7090 is also found to show a new type of binding kinetics to FGFR1 with fast association and slow dissociation.

Table 1. Parameters of kinetic interactions with FGFR1.

	IC_{50} (nmol/L)	Kd (nmol/L)	Kon ($s^{-1} \times M^{-1}$)	Koff (s^{-1})	Residence time (min)
E7090 succinate	5.00 ± 0.15	2.50 ± 0.08	3.43×10^{5} $\pm 4.78 \times 10^{4}$	8.57×10^{-4} $\pm 1.45 \times 10^{-4}$	19 ± 3
AZD4547	6.02 ± 0.22	3.01 ± 0.11	7.51×10^{5} $\pm 1.19 \times 10^{5}$	2.26×10^{-3} $\pm 4.43 \times 10^{-4}$	7 ± 1
Ponatinib	22.4 ± 1.30	11.2 ± 0.65	2.62×10^{4} $\pm 1.11 \times 10^{3}$	2.93×10^{-4} $\pm 2.93 \times 10^{-5}$	57 ± 6

Kd = 1/2 × IC_{50}, K_{off} = KD × K_{on}, residence time = $1/K_{off}$

Table 2

Antitumor activity of E7090 or E7090 succinate in various mouse models implanted with human cancer cell lines.

Cell line	Tissue	FGFRs abnormality	Dosing duration (days)	⊿ T/C (%)			
				6.25 mg/kg	12.5 mg/kg	25 mg/kg	50 mg/kg
SNU-16#	Gastric	*FGFR2* amplification	14	51*	26*	13*	0*
NCI-H1581#	Lung	*FGFR1* amplification	14	37*	17*	5*	1*
DMS114	Lung	*FGFR1* amplification	14	NT	61	44*	38*
RT112/84	Bladder	FGFR3-TACC3 fusion	14	48	61	41	-5*
MFM223#	Breast	*FGFR1&2* amplification	12	NT	-2*	NT	-42*
HCC1806#	Breast	None	11	NT	NT	NT	93
MCF7#	Breast	None	14	NT	NT	NT	104
HCC1428#	Breast	None	14	NT	NT	NT	103
MDA-MB-468#	Breast	None	14	NT	NT	NT	97

NT: not tested, #:E7090 succinate data, *:$P < 0.05$ (Dunnett test vs vehicle at last dosing day)

Table 3. Median survival time of each treated group in 4T1 lung metastasis model.

	Median Survival Time (days)	Survival (% of control)	P value
Vehicle	19	100	
6.25 mg/kg	22	116	0.0797
12.5 mg/kg	23	121*	0.0018
25 mg/kg	29	150*	<0.0001
50 mg/kg	34	176*	<0.0001

* $P < 0.05$ compared with vehicle-treated mice (Log-rank (Mantel-Cox) test)

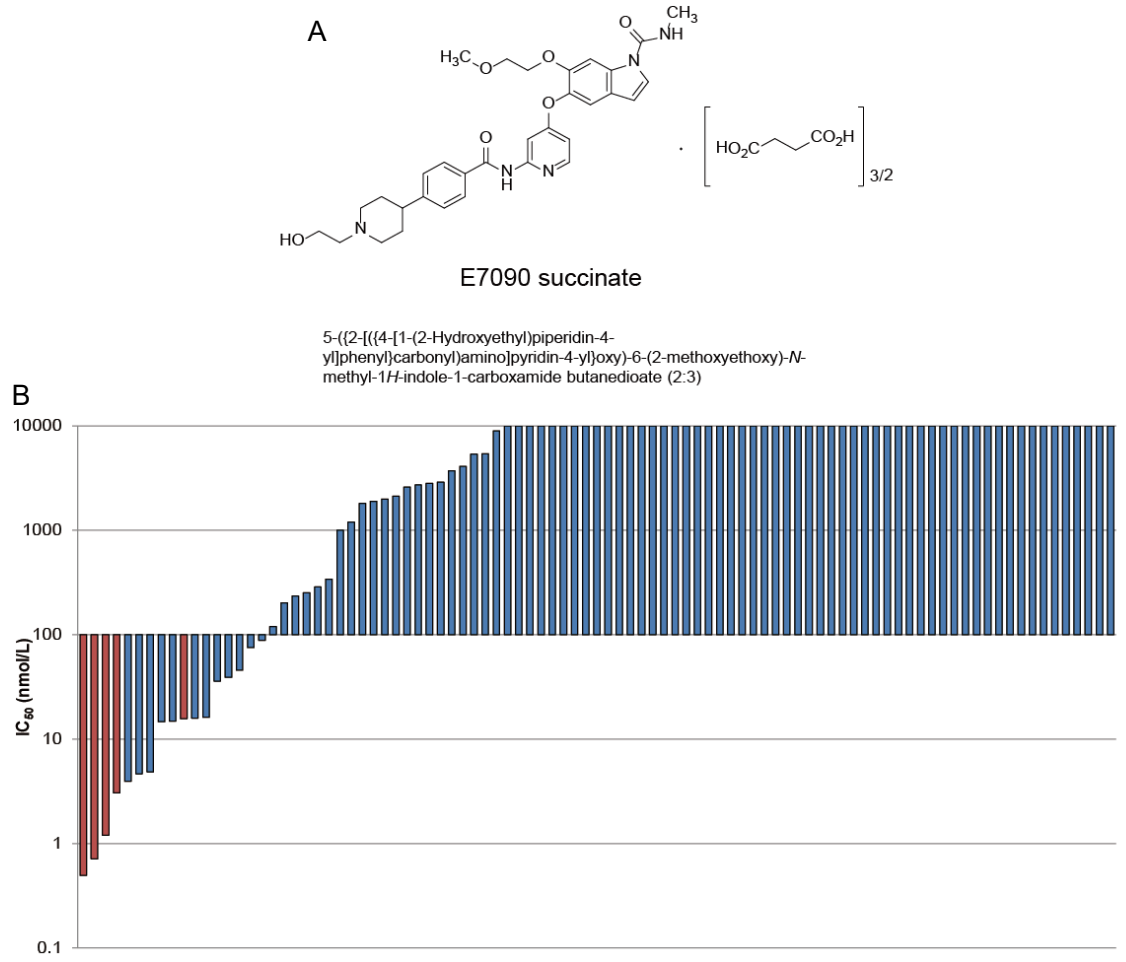

Figure 1. The chemical structure of E7090 succinate and the selectivity against 93 kinases with E7090.

A, Chemical structure of E7090 succinate, 5-({2-[({4-[1-(2-Hydroxyethyl)piperidin-4-yl]phenyl}carbonyl)amino]pyridin-4-yl}oxy)-6-(2-methoxyethoxy)-*N*-methyl-1*H*-indole-1-carboxamide butanedioate (2:3).

B, IC_{50} values for the inhibition by E7090 of 93 human kinases. Bars that indicate wild-type or mutated FGFR1, -2, or -3 are shown in red. See Supplementary Table S1 for the full list.

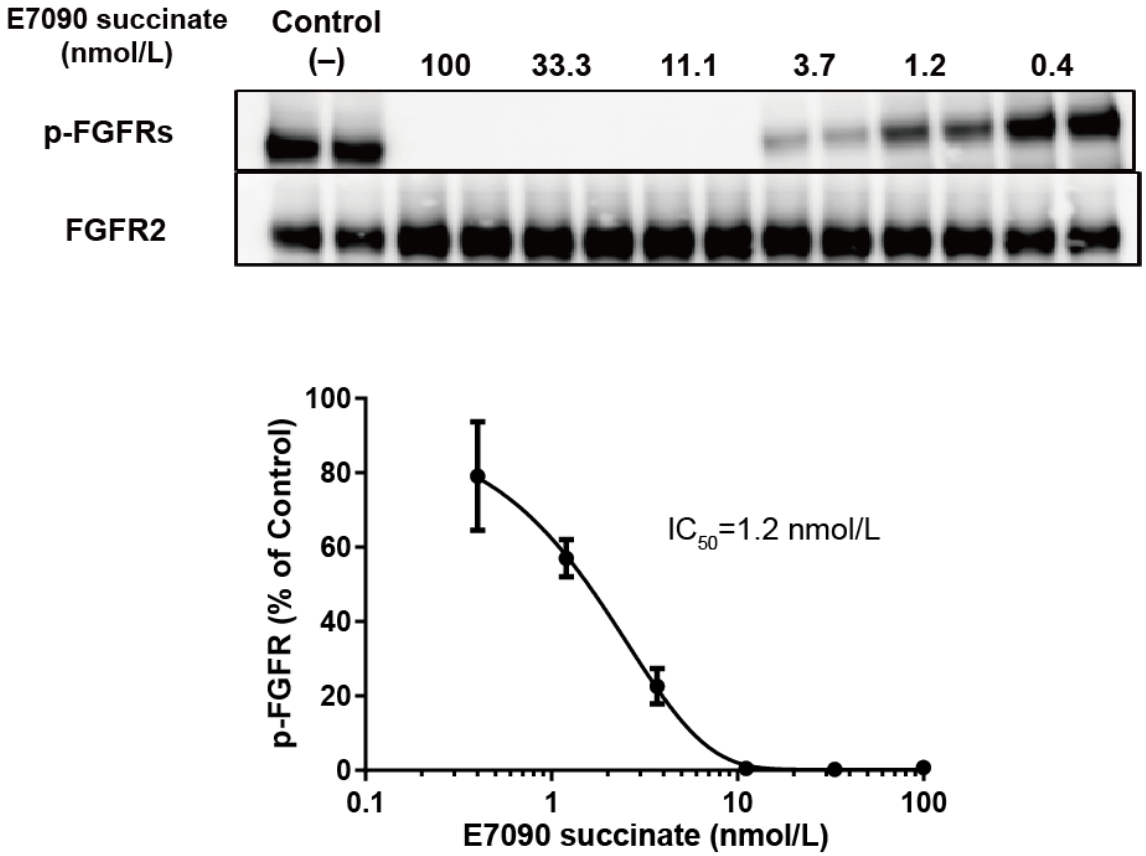

Figure 2. Inhibition of FGFRs phosphorylation by E7090 in human gastric cancer cell line SNU-16.

Effect of E7090 succinate on phosphorylation of FGFR in SNU-16 cells. Cells were treated for 4 h, and whole-cell lysates were analyzed by Western blotting with antibodies to phospho-FGFR (p-FGFR; Y653/654) or FGFR2. Band intensity was quantified and the IC_{50} value was calculated. Data are shown as mean ± SD (n = 3).

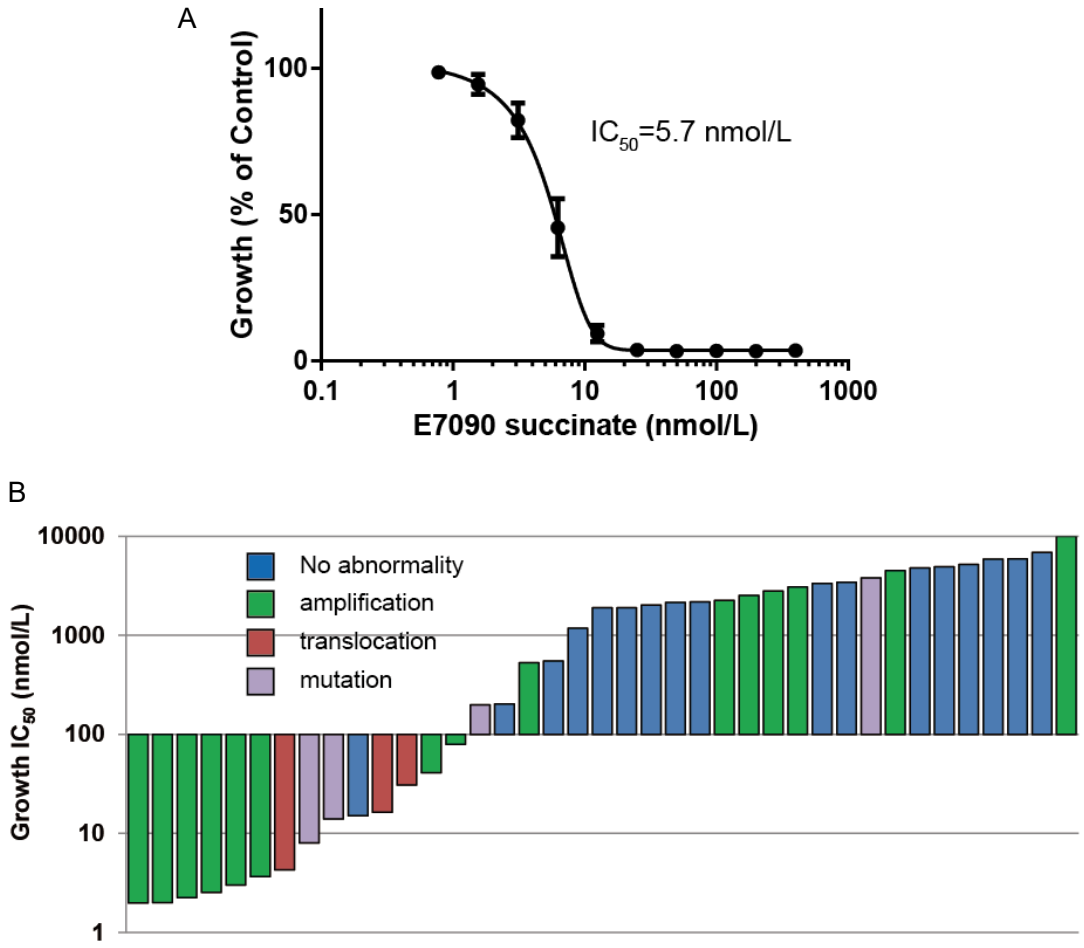

Figure 3. Inhibition of cell proliferation by E7090 in human cancer cell lines.
A, SNU-16 cells were incubated with the indicated concentrations of E7090 succinate for 72 h, and IC_{50} values were calculated. Data are shown as mean ± SD (n = 3).
B, Cells were treated with various concentrations of E7090 and cell growth was measured by Cell Counting Kit-8. Cell lines are shown in order of IC_{50} values and categorized by FGFR gene alterations. Detailed information, including IC_{50} value and incubation time, is shown in Supplementary Table S2.

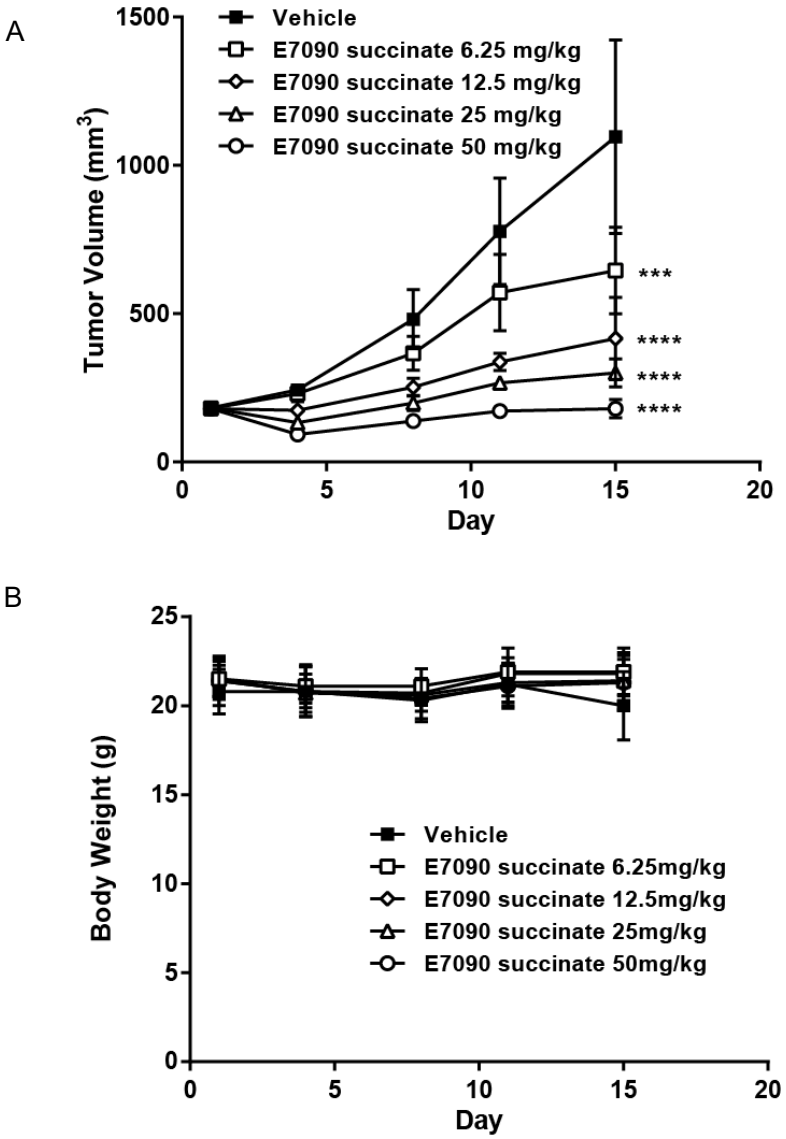

Figure 4. Inhibition of tumor growth in SNU-16 xenograft model by administration of E7090.

Nude mice bearing SNU-16 xenografts were treated orally once daily for 14 days with either vehicle or E7090 succinate at the indicated doses.

A, Tumor volume. Data are shown as mean ± SD (n = 6). ***, $P < 0.001$, ****, $P < 0.0001$ compared with vehicle-treated mice (Dunnett test).

B, Body weight measurements during the treatment. Data are shown as mean ± SD (n = 6).

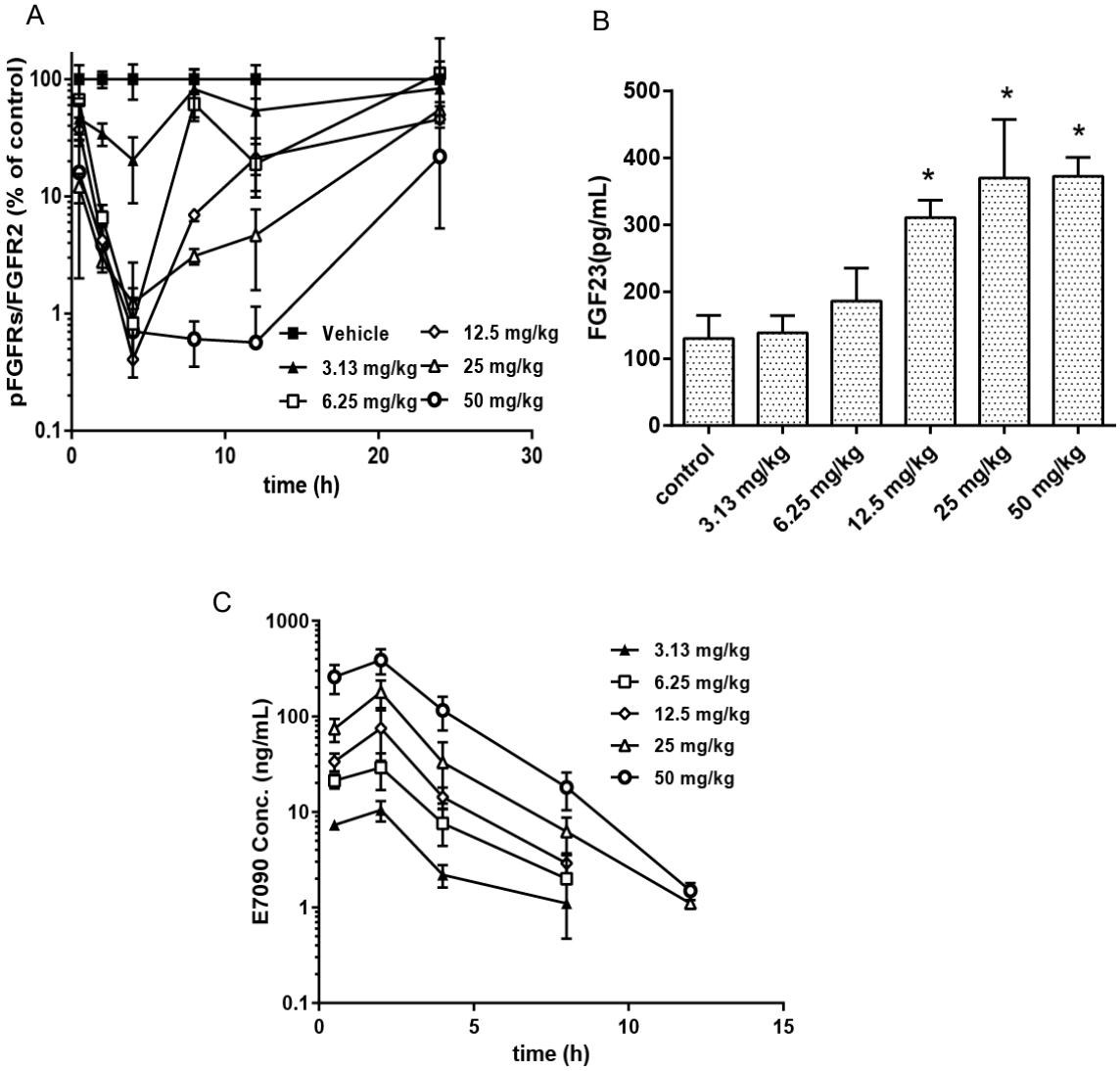

Figure 5. Inhibition of FGFR signaling in SNU-16 xenograft model by administration of E7090.

A, Pharmacodynamic analysis of E7090 in mice bearing SNU-16 tumors. E7090 was orally administered at the indicated doses, and blood and tumors were collected at the indicated time points. The percentage of FGFR2 phosphorylation compared with vehicle is plotted. Data are shown as mean ± SD (E7090: n = 3; vehicle: n = 5). Western blotting data for each sample against FGFR2 or phospho-FGFR (Y653/654) are also shown in Supplementary Figure S3.

B. Plasma FGF23 level 24 h after administration of E7090 or vehicle (control). FGF23 concentrations were determined by ELISA from plasma. Data are shown as mean ± SD. *, $P < 0.05$ compared with vehicle-treated mice (Dunnett test).

C, Pharmacokinetic analysis of E7090 in mice bearing SNU-16 tumors. E7090 was orally administered at the indicated doses, and blood and tumors were collected at the indicated time points. E7090 concentration in plasma is plotted.

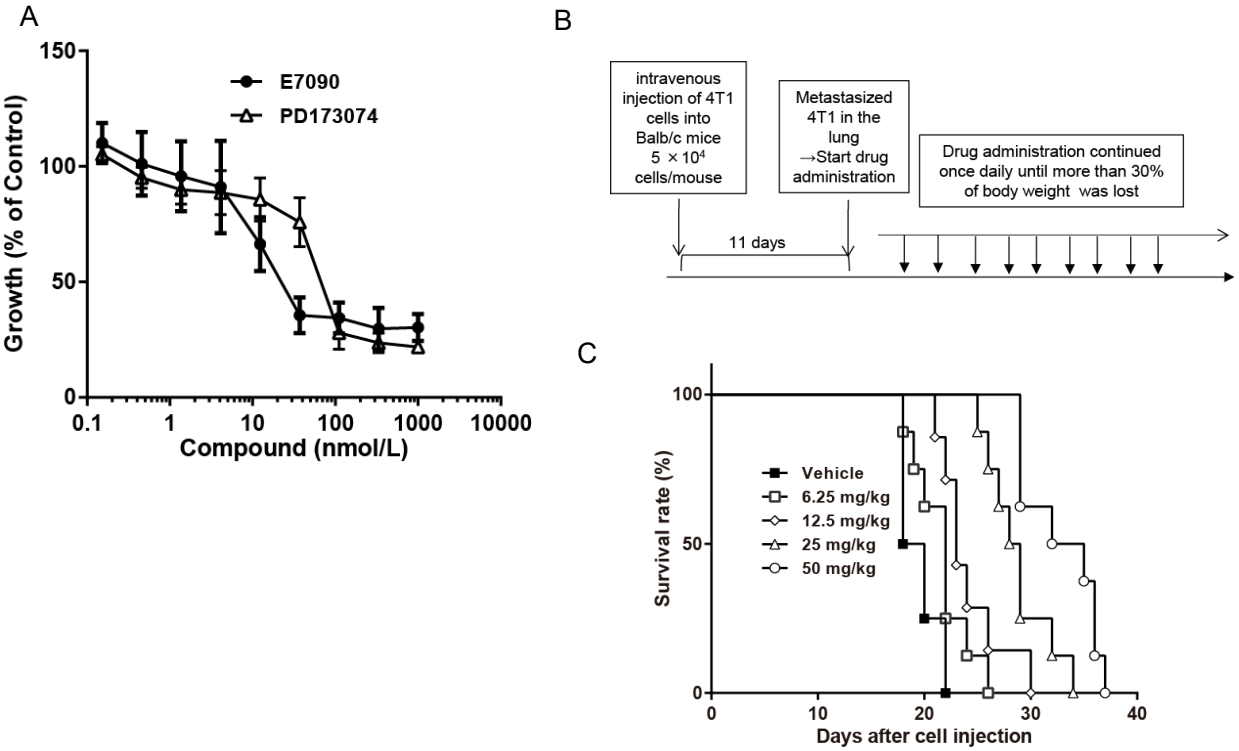

Figure 6. Prolonged survival with daily E7090 administration in a mouse 4T1 lung metastasis model.

A. Both E7090 and PD173074 show inhibitory activity against the growth of 4T1 cells. 4T1 cells were incubated with the indicated concentrations of E7090 or PD173074 for 72 h. Data are presented as mean ± SD (n = 3).

B. Experimental plan for the 4T1 lung metastasis model.

C. Survival curve of 4T1 lung metastasis model. Cultured 4T1 cells were inoculated intravenously into Balb/c mice on day 0. Daily administration with either vehicle or E7090 was started on day 11. Each group comprised 8 mice.

Supplementary information

Supplementary Table S1

IC_{50} values for the inhibition of 93 human kinases by E7090.

kinase	IC_{50} (nmol/L)	kinase	IC_{50} (nmol/L)	kinase	IC_{50} (nmol/L)	kinase	IC_{50} (nmol/L)
FGFR1	0.71	FRK	340	INSR	>10000	Erk2	>10000
FGFR2	0.50	HER4	1000	JAK2	>10000	GSK3β	>10000
FGFR3	1.2	BRK	1200	KIT(D816V)	>10000	IKKβ	>10000
FGFR4	120	BRAF(V600E)_Cascade	1800	KIT(T670I)	>10000	IRAK4	>10000
FGFR3(K650E)	3.1	SRC	1900	MET	>10000	JNK2	>10000
FGFR3(K650M)	16	EPHA1	2000	MUSK	>10000	MAPKAPK2	>10000
FGFR4(N535K)	88	EPHB2	2100	ROS	>10000	MST1	>10000
FGFR4(V550E)	>10000	CSK	2600	SYK	>10000	NEK2	>10000
FGFR4(V550L)	>10000	PDGFRα(T674I)	2700	TRKB	>10000	p70S6K	>10000
RET	3.9	p38α	2800	AKT1	>10000	PAK2	>10000
DDR2	4.7	RAF1_Cascade	2900	AMPKα1/β1/γ1	>10000	PBK	>10000
FLT1	4.9	HGK	3700	AurA	>10000	PDK1	>10000
RET(M918T)	15	TIE2	4100	BRAF_Cascade	>10000	PIM1	>10000
PDGFRα	15	EPHB4	5400	CaMK4	>10000	PKACα	>10000
FLT4	16	MLK1_Cascade	5400	CDK2/CycA2	>10000	PKCα	>10000
KDR	16	EGFR	9000	CDK2/CycE1	>10000	PKD2	>10000
LYNa	36	ALK	>10000	CDK4/CycD3	>10000	PLK1	>10000
PDGFRβ	39	AXL	>10000	CDK6/CycD3	>10000	PRKX	>10000
LYNb	46	EPHB3	>10000	CHK1	>10000	ROCK2	>10000
YES	75	FAK	>10000	CK1ε	>10000	SGK3	>10000
FGR	200	FLT3	>10000	COT_Cascade	>10000	TSSK1	>10000
KIT	240	HER2	>10000	DAPK1	>10000	PIK3CA/PIK3R1	>10000
ABL	250	IGF1R	>10000	DYRK1B	>10000		
LCK	290	KIT(V654A)	>10000				

Supplementary Table S2

IC_{50} values for growth inhibition of various cancer cell lines by E7090.

Cell line	IC_{50} (nmol/L)	Incubation time (days)	Cell line	IC_{50} (nmol/L)	Incubation time (days)
MFM223	2.0	3	T47D	1900	3
MDA-MB-134	2.0	13	PC9	2000	6
NCI-H1581	2.2	6	MKN-74	2100	3
HSC-39	2.5	3	SNU-5	2200	3
SNU-16	3.0	3	NCI-H2444	2300	6
KATO-III	3.7	3	DMS454	2500	6
KG-1a	4.0	3	CORL88	2800	6
KMS-11	8.0	6	NCI-H1703	3100	6
MFE-280	14	3	HCC827	3300	6
A427	15	6	MKN-45	3400	3
RT4	16	3	J82	3800	3
RT112/84	31	3	CAMA-1	4500	3
NCI-H520	41	6	NCI-H1650	4800	6
DMS114	79	6	MKN-1	4900	3
OPM-2	200	6	A549	5200	6
BT474	200	3	Hs746T	5900	3
ZR-75-1	530	3	MCF-7	5900	3
DU4475	550	3	MKN-7	6900	3
HT1197	1200	3	CAL120	>10000	3
NCI-H226	1900	6			

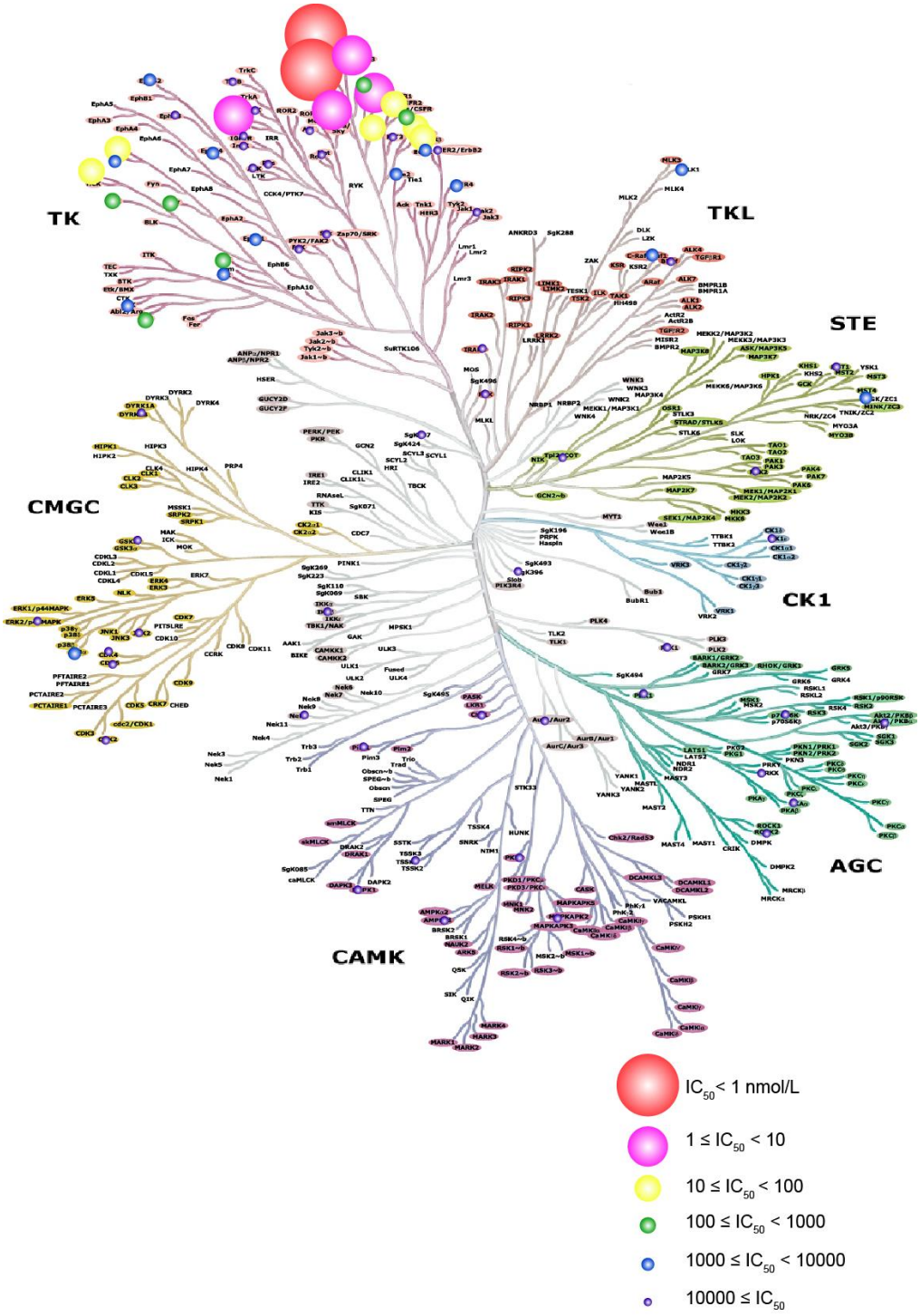

Supplementary Figure S1

Kinome map of E7090.

IC50 values of E7090 against wild-type kinases were used to create this kinome map. Illustration reproduced courtesy of Cell Signaling Technology, Inc. (www.cellsignal.com).

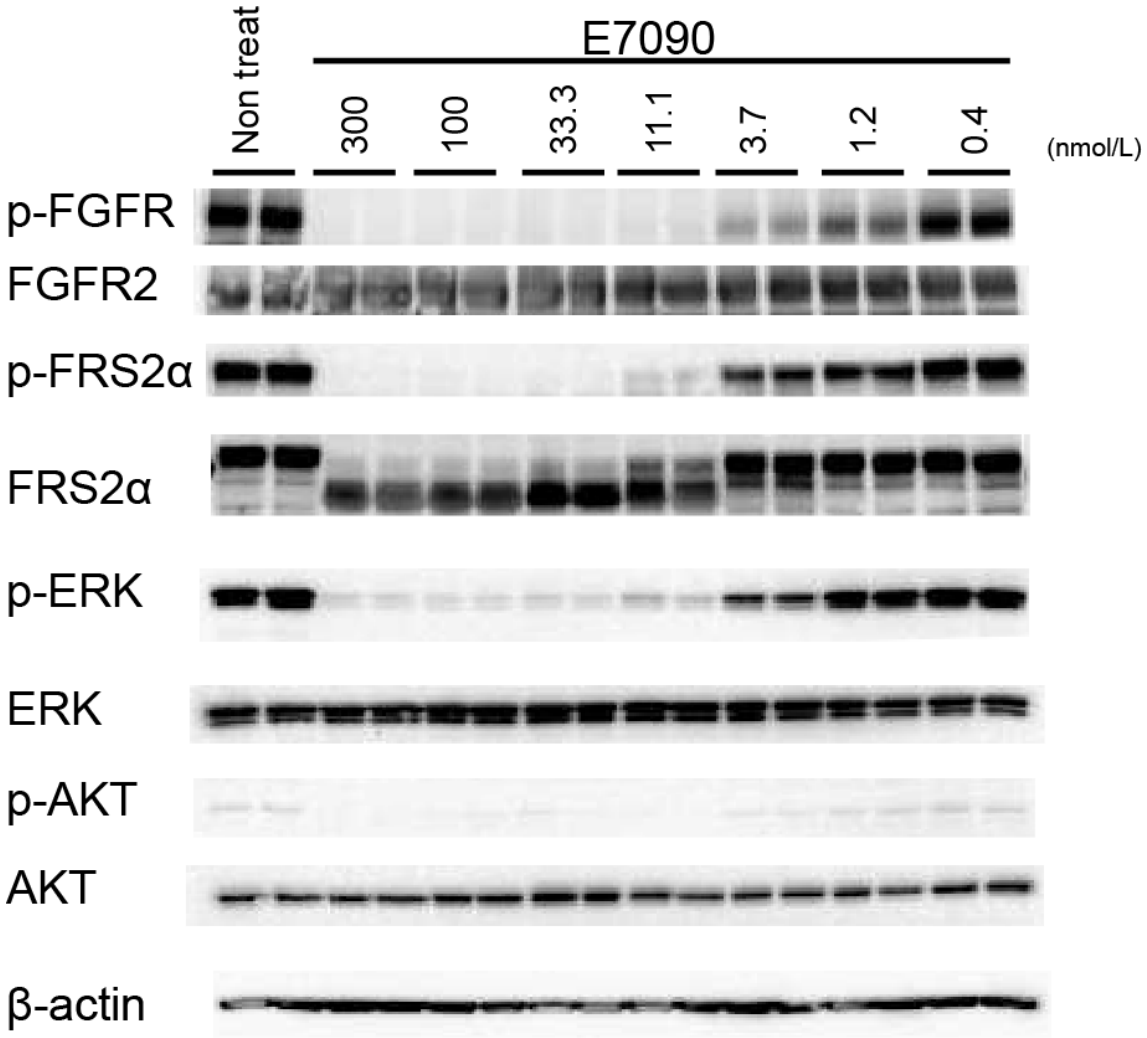

Supplementary Figure S2

Inhibition of expression of proteins downstream of FGFR, including FRS2α, ERK, and AKT, in SNU-16 cells in vitro.

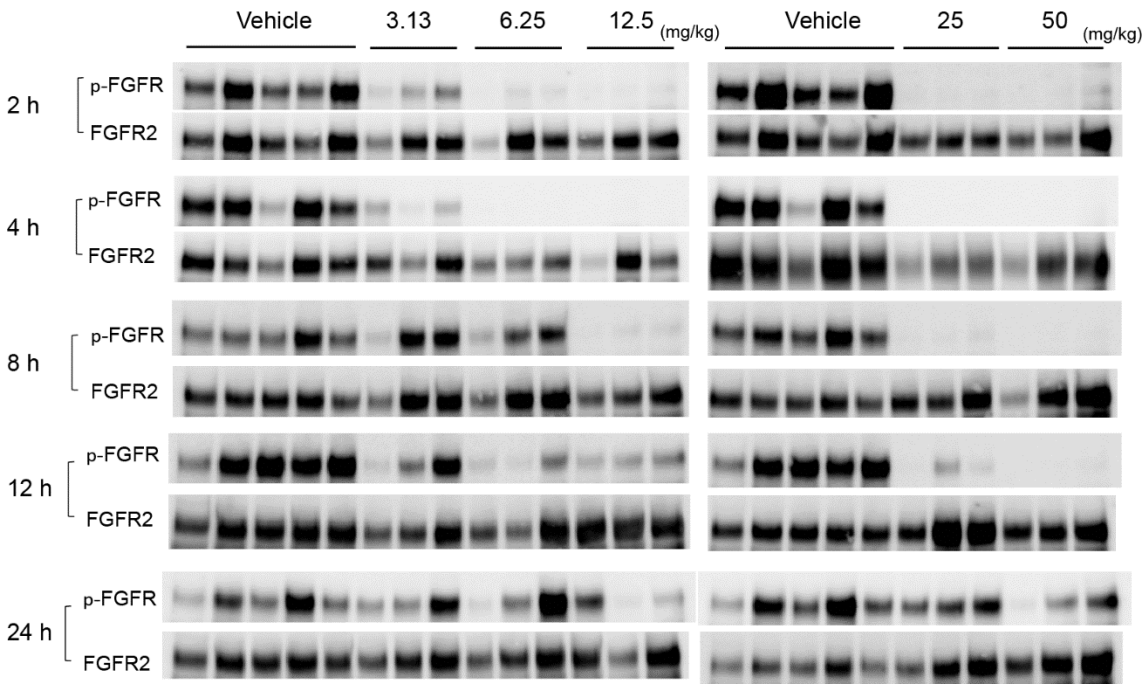

Supplementary Figure S3

Western blot analysis of phospho-FGFR in SNU-16 tumors at the indicated times after treatment with the indicated concentrations of E7090. See also Figure 5A.

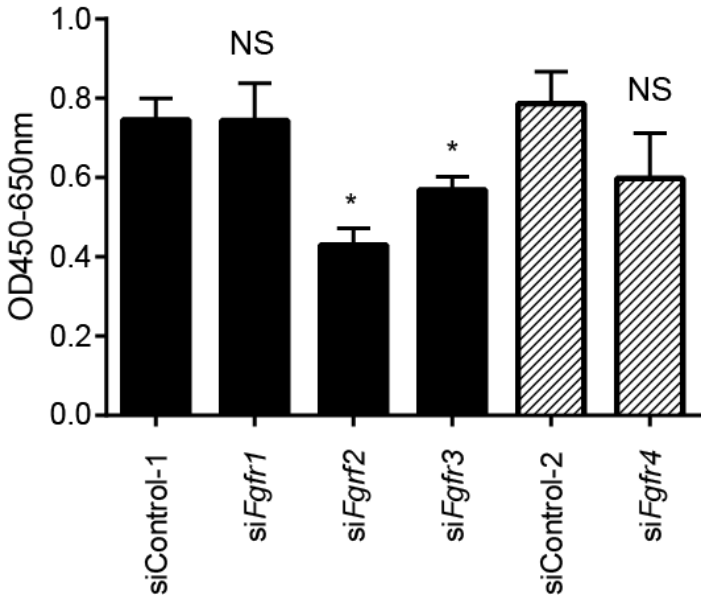

Supplementary Figure S4

siRNA knockdown experiment in 4T1 cells indicating that growth of 4T1 breast cancer cells depends on FGFR2 and FGFR3. *, $P < 0.05$ compared with siControl-treated cells (Dunnett test (vs si*Fgfr1*, si*Fgfr2* and si*Fgfr3*) or t-test (vs si*Fgfr4*)).

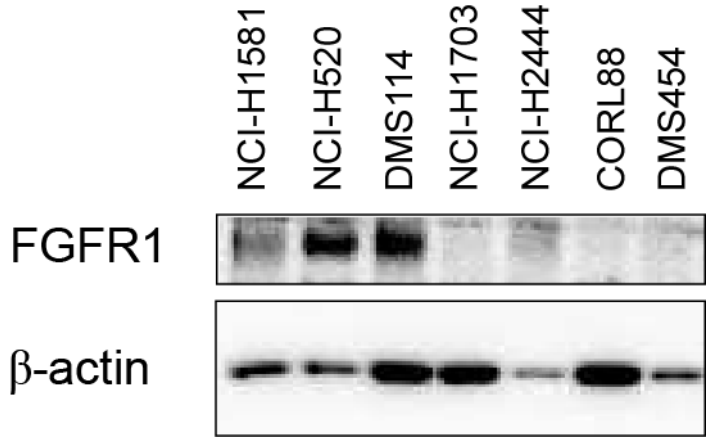

Supplementary Figure S5
Western blot analysis of FGFR1 in human lung cancer cell lines harboring *FGFR1* amplifications.

References

Andre, F., and Cortes, J. (2015). Rationale for targeting fibroblast growth factor receptor signaling in breast cancer. Breast Cancer Res Treat *150*, 1-8.

Arai, Y., Totoki, Y., Hosoda, F., Shirota, T., Hama, N., Nakamura, H., Ojima, H., Furuta, K., Shimada, K., Okusaka, T.*, et al.* (2014). Fibroblast growth factor receptor 2 tyrosine kinase fusions define a unique molecular subtype of cholangiocarcinoma. Hepatology *59*, 1427-1434.

Bailey-Downs, L.C., Thorpe, J.E., Disch, B.C., Bastian, A., Hauser, P.J., Farasyn, T., Berry, W.L., Hurst, R.E., and Ihnat, M.A. (2014). Development and Characterization of a Preclinical Model of Breast Cancer Lung Micrometastatic to Macrometastatic Progression. PLOS ONE *9*, e98624.

Barretina, J., Caponigro, G., Stransky, N., Venkatesan, K., Margolin, A.A., Kim, S., Wilson, C.J., Lehar, J., Kryukov, G.V., Sonkin, D.*, et al.* (2012). The Cancer Cell Line Encyclopedia enables predictive modelling of anticancer drug sensitivity. Nature *483*, 603-607.

Branford, S., Rudzki, Z., Walsh, S., Grigg, A., Arthur, C., Taylor, K., Herrmann, R., Lynch, K.P., and Hughes, T.P. (2002). High frequency of point mutations clustered within the adenosine triphosphate-binding region of BCR/ABL in patients with chronic myeloid leukemia or Ph-positive acute lymphoblastic leukemia who develop imatinib (STI571) resistance. Blood *99*, 3472-3475.

Byron, S.A., Chen, H., Wortmann, A., Loch, D., Gartside, M.G., Dehkhoda, F., Blais, S.P., Neubert, T.A., Mohammadi, M., and Pollock, P.M. (2013). The N550K/H Mutations in FGFR2 Confer Differential Resistance to PD173074, Dovitinib, and Ponatinib ATP-Competitive Inhibitors. Neoplasia *15*, 975-IN930.

Byron, S.A., Gartside, M., Powell, M.A., Wellens, C.L., Gao, F., Mutch, D.G., Goodfellow, P.J., and Pollock, P.M. (2012). FGFR2 point mutations in 466 endometrioid endometrial tumors: relationship with MSI, KRAS, PIK3CA, CTNNB1 mutations and clinicopathological features. PLoS One *7*, e30801.

Cancer Genome Atlas Research, N. (2012). Comprehensive genomic characterization of

squamous cell lung cancers. Nature *489*, 519-525.

Carter, E.P., Fearon, A.E., and Grose, R.P. (2015). Careless talk costs lives: fibroblast growth factor receptor signalling and the consequences of pathway malfunction. Trends Cell Biol *25*, 221-233.

Chell, V., Balmanno, K., Little, A.S., Wilson, M., Andrews, S., Blockley, L., Hampson, M., Gavine, P.R., and Cook, S.J. (2013). Tumour cell responses to new fibroblast growth factor receptor tyrosine kinase inhibitors and identification of a gatekeeper mutation in FGFR3 as a mechanism of acquired resistance. Oncogene *32*, 3059-3070.

Dey, J.H., Bianchi, F., Voshol, J., Bonenfant, D., Oakeley, E.J., and Hynes, N.E. (2010). Targeting fibroblast growth factor receptors blocks PI3K/AKT signaling, induces apoptosis, and impairs mammary tumor outgrowth and metastasis. Cancer Res *70*, 4151-4162.

Dieci, M.V., Arnedos, M., Andre, F., and Soria, J.C. (2013). Fibroblast growth factor receptor inhibitors as a cancer treatment: from a biologic rationale to medical perspectives. Cancer Discov *3*, 264-279.

Dutt, A., Ramos, A.H., Hammerman, P.S., Mermel, C., Cho, J., Sharifnia, T., Chande, A., Tanaka, K.E., Stransky, N., Greulich, H.*, et al.* (2011). Inhibitor-sensitive FGFR1 amplification in human non-small cell lung cancer. PLoS One *6*, e20351.

Gallo, L.H., Nelson, K.N., Meyer, A.N., and Donoghue, D.J. (2015). Functions of Fibroblast Growth Factor Receptors in cancer defined by novel translocations and mutations. Cytokine Growth Factor Rev *26*, 425-449.

Gavine, P.R., Mooney, L., Kilgour, E., Thomas, A.P., Al-Kadhimi, K., Beck, S., Rooney, C., Coleman, T., Baker, D., Mellor, M.J.*, et al.* (2012). AZD4547: an orally bioavailable, potent, and selective inhibitor of the fibroblast growth factor receptor tyrosine kinase family. Cancer Res *72*, 2045-2056.

Guagnano, V., Furet, P., Spanka, C., Bordas, V., Le Douget, M., Stamm, C., Brueggen, J., Jensen, M.R., Schnell, C., Schmid, H.*, et al.* (2011). Discovery of 3-(2,6-dichloro-3,5-dimethoxy-phenyl)-1-{6-[4-(4-ethyl-piperazin-1-yl)-phenylamin o]-pyrimidin-4-yl}-1-methyl-

urea (NVP-BGJ398), a potent and selective inhibitor of the fibroblast growth factor receptor family of receptor tyrosine kinase. J Med Chem *54*, 7066-7083.

Ichikawa K, M.S., Adachi Y, Matsuki M, Okamoto K, ., and et al. (2016). Lenvatinib Suppresses Angiogenesis through the Inhibition of both the VEGFR and FGFR Signaling Pathways. Glob J Cancer Ther *2*, 019-024.

Kim, K.B., Chesney, J., Robinson, D., Gardner, H., Shi, M.M., and Kirkwood, J.M. (2011). Phase I/II and pharmacodynamic study of dovitinib (TKI258), an inhibitor of fibroblast growth factor receptors and VEGF receptors, in patients with advanced melanoma. Clin Cancer Res *17*, 7451-7461.

Kotani, H., Ebi, H., Kitai, H., Nanjo, S., Kita, K., Huynh, T.G., Ooi, A., Faber, A.C., Mino-Kenudson, M., and Yano, S. (2016). Co-active receptor tyrosine kinases mitigate the effect of FGFR inhibitors in FGFR1-amplified lung cancers with low FGFR1 protein expression. Oncogene *35*, 3587-3597.

Kunii, K., Davis, L., Gorenstein, J., Hatch, H., Yashiro, M., Di Bacco, A., Elbi, C., and Lutterbach, B. (2008). FGFR2-amplified gastric cancer cell lines require FGFR2 and Erbb3 signaling for growth and survival. Cancer Res *68*, 2340-2348.

Lamont, F.R., Tomlinson, D.C., Cooper, P.A., Shnyder, S.D., Chester, J.D., and Knowles, M.A. (2011). Small molecule FGF receptor inhibitors block FGFR-dependent urothelial carcinoma growth in vitro and in vivo. Br J Cancer *104*, 75-82.

Li, Y., Shen, M., Zhang, Z., Luo, J., Pan, X., Lu, X., Long, H., Wen, D., Zhang, F., Leng, F.*, et al.* (2012). Design, synthesis, and biological evaluation of 3-(1H-1,2,3-triazol-1-yl)benzamide derivatives as Potent Pan Bcr-Abl inhibitors including the threonine(315)-->isoleucine(315) mutant. J Med Chem *55*, 10033-10046.

Liao, R.G., Jung, J., Tchaicha, J., Wilkerson, M.D., Sivachenko, A., Beauchamp, E.M., Liu, Q., Pugh, T.J., Pedamallu, C.S., Hayes, D.N.*, et al.* (2013). Inhibitor-sensitive FGFR2 and FGFR3 mutations in lung squamous cell carcinoma. Cancer Res *73*, 5195-5205.

Liu, Y., and Gray, N.S. (2006). Rational design of inhibitors that bind to inactive kinase

conformations. Nat Chem Biol *2*, 358-364.

Malchers, F., Dietlein, F., Schottle, J., Lu, X., Nogova, L., Albus, K., Fernandez-Cuesta, L., Heuckmann, J.M., Gautschi, O., Diebold, J.*, et al.* (2014). Cell-autonomous and non-cell-autonomous mechanisms of transformation by amplified FGFR1 in lung cancer. Cancer Discov *4*, 246-257.

Matsumoto, K., Arao, T., Hamaguchi, T., Shimada, Y., Kato, K., Oda, I., Taniguchi, H., Koizumi, F., Yanagihara, K., Sasaki, H.*, et al.* (2012). FGFR2 gene amplification and clinicopathological features in gastric cancer. Br J Cancer *106*, 727-732.

Mohammadi, M., Froum, S., Hamby, J.M., Schroeder, M.C., Panek, R.L., Lu, G.H., Eliseenkova, A.V., Green, D., Schlessinger, J., and Hubbard, S.R. (1998). Crystal structure of an angiogenesis inhibitor bound to the FGF receptor tyrosine kinase domain. EMBO J *17*, 5896-5904.

Network, C.G.A.R. (2014). Comprehensive molecular characterization of urothelial bladder carcinoma. Nature *507*, 315-322.

Neumann, L., Ritscher, A., Muller, G., and Hafenbradl, D. (2009). Fragment-based lead generation: identification of seed fragments by a highly efficient fragment screening technology. J Comput Aided Mol Des *23*, 501-511.

Neumann, L., von Konig, K., and Ullmann, D. (2011). HTS reporter displacement assay for fragment screening and fragment evolution toward leads with optimized binding kinetics, binding selectivity, and thermodynamic signature. Methods Enzymol *493*, 299-320.

Okamoto, K., Ikemori-Kawada, M., Jestel, A., von Konig, K., Funahashi, Y., Matsushima, T., Tsuruoka, A., Inoue, A., and Matsui, J. (2015). Distinct binding mode of multikinase inhibitor lenvatinib revealed by biochemical characterization. ACS Med Chem Lett *6*, 89-94.

Procopio, M.-G., Laszlo, C., Al Labban, D., Kim, D.E., Bordignon, P., Jo, S.-H., Goruppi, S., Menietti, E., Ostano, P., Ala, U.*, et al.* (2015). Combined CSL and p53 downregulation promotes cancer-associated fibroblast activation. Nat Cell Biol *17*, 1193-1204.

Ramos, A.H., Dutt, A., Mermel, C., Perner, S., Cho, J., Lafargue, C.J., Johnson, L.A., Stiedl,

A.C., Tanaka, K.E., Bass, A.J., *et al.* (2009). Amplification of chromosomal segment 4q12 in non-small cell lung cancer. Cancer Biol Ther *8*, 2042-2050.

Rashid, O.M., Nagahashi, M., Ramachandran, S., Dumur, C., Schaum, J., Yamada, A., Terracina, K.P., Milstien, S., Spiegel, S., and Takabe, K. (2014). An improved syngeneic orthotopic murine model of human breast cancer progression. Breast Cancer Res Treat *147*, 501-512.

Singh, D., Chan, J.M., Zoppoli, P., Niola, F., Sullivan, R., Castano, A., Liu, E.M., Reichel, J., Porrati, P., Pellegatta, S., *et al.* (2012). Transforming fusions of FGFR and TACC genes in human glioblastoma. Science *337*, 1231-1235.

Sohl, C.D., Ryan, M.R., Luo, B., Frey, K.M., and Anderson, K.S. (2015). Illuminating the molecular mechanisms of tyrosine kinase inhibitor resistance for the FGFR1 gatekeeper mutation: the Achilles' heel of targeted therapy. ACS Chem Biol *10*, 1319-1329.

Sutto, L., and Gervasio, F.L. (2013). Effects of oncogenic mutations on the conformational free-energy landscape of EGFR kinase. Proc Natl Acad Sci U S A *110*, 10616-10621.

Suyama, K., Shapiro, I., Guttman, M., and Hazan, R.B. (2002). A signaling pathway leading to metastasis is controlled by N-cadherin and the FGF receptor. Cancer Cell *2*, 301-314.

Tabernero, J., Bahleda, R., Dienstmann, R., Infante, J.R., Mita, A., Italiano, A., Calvo, E., Moreno, V., Adamo, B., Gazzah, A., *et al.* (2015). Phase I Dose-Escalation Study of JNJ-42756493, an Oral Pan-Fibroblast Growth Factor Receptor Inhibitor, in Patients With Advanced Solid Tumors. J Clin Oncol *33*, 3401-3408.

Thomas, A., Lee, J.H., Abdullaev, Z., Park, K.S., Pineda, M., Saidkhodjaeva, L., Miettinen, M., Wang, Y., Pack, S.D., and Giaccone, G. (2014). Characterization of fibroblast growth factor receptor 1 in small-cell lung cancer. J Thorac Oncol *9*, 567-571.

Thompson, A.M., Delaney, A.M., Hamby, J.M., Schroeder, M.C., Spoon, T.A., Crean, S.M., Showalter, H.D., and Denny, W.A. (2005). Synthesis and structure-activity relationships of soluble 7-substituted 3-(3,5-dimethoxyphenyl)-1,6-naphthyridin-2-amines and related ureas as dual inhibitors of the fibroblast growth factor receptor-1 and vascular endothelial growth

factor receptor-2 tyrosine kinases. J Med Chem *48*, 4628-4653.

Tucker, J.A., Klein, T., Breed, J., Breeze, A.L., Overman, R., Phillips, C., and Norman, R.A. (2014). Structural insights into FGFR kinase isoform selectivity: diverse binding modes of AZD4547 and ponatinib in complex with FGFR1 and FGFR4. Structure *22*, 1764-1774.

Tummino, P.J., and Copeland, R.A. (2008). Residence Time of Receptor−Ligand Complexes and Its Effect on Biological Function. Biochemistry *47*, 5481-5492.

Turner, N., and Grose, R. (2010). Fibroblast growth factor signalling: from development to cancer. Nat Rev Cancer *10*, 116-129.

Turner, N., Pearson, A., Sharpe, R., Lambros, M., Geyer, F., Lopez-Garcia, M.A., Natrajan, R., Marchio, C., Iorns, E., Mackay, A.*, et al.* (2010). FGFR1 amplification drives endocrine therapy resistance and is a therapeutic target in breast cancer. Cancer Res *70*, 2085-2094.

Weiss, J., Sos, M.L., Seidel, D., Peifer, M., Zander, T., Heuckmann, J.M., Ullrich, R.T., Menon, R., Maier, S., Soltermann, A.*, et al.* (2010). Frequent and focal FGFR1 amplification associates with therapeutically tractable FGFR1 dependency in squamous cell lung cancer. Sci Transl Med *2*, 62ra93.

WERNER, S., and GROSE, R. (2003). Regulation of Wound Healing by Growth Factors and Cytokines. Physiological Reviews *83*, 835-870.

Williams, S.V., Hurst, C.D., and Knowles, M.A. (2013). Oncogenic FGFR3 gene fusions in bladder cancer. Hum Mol Genet *22*, 795-803.

Wohrle, S., Bonny, O., Beluch, N., Gaulis, S., Stamm, C., Scheibler, M., Muller, M., Kinzel, B., Thuery, A., Brueggen, J.*, et al.* (2011). FGF receptors control vitamin D and phosphate homeostasis by mediating renal FGF-23 signaling and regulating FGF-23 expression in bone. J Bone Miner Res *26*, 2486-2497.

Wu, P., Nielsen, T.E., and Clausen, M.H. (2016). Small-molecule kinase inhibitors: an analysis of FDA-approved drugs. Drug Discov Today *21*, 5-10.

Wu, Y.M., Su, F., Kalyana-Sundaram, S., Khazanov, N., Ateeq, B., Cao, X., Lonigro, R.J., Vats, P., Wang, R., Lin, S.F.*, et al.* (2013). Identification of targetable FGFR gene fusions in diverse

cancers. Cancer Discov *3*, 636-647.

Xie, L., Su, X., Zhang, L., Yin, X., Tang, L., Zhang, X., Xu, Y., Gao, Z., Liu, K., Zhou, M.*, et al.* (2013). FGFR2 gene amplification in gastric cancer predicts sensitivity to the selective FGFR inhibitor AZD4547. Clin Cancer Res *19*, 2572-2583.

Yamazaki, S., Vicini, P., Shen, Z., Zou, H.Y., Lee, J., Li, Q., Christensen, J.G., Smith, B.J., and Shetty, B. (2012). Pharmacokinetic/pharmacodynamic modeling of crizotinib for anaplastic lymphoma kinase inhibition and antitumor efficacy in human tumor xenograft mouse models. J Pharmacol Exp Ther *340*, 549-557.

Yun, C.H., Mengwasser, K.E., Toms, A.V., Woo, M.S., Greulich, H., Wong, K.K., Meyerson, M., and Eck, M.J. (2008). The T790M mutation in EGFR kinase causes drug resistance by increasing the affinity for ATP. Proc Natl Acad Sci U S A *105*, 2070-2075.

Zhou, T., Parillon, L., Li, F., Wang, Y., Keats, J., Lamore, S., Xu, Q., Shakespeare, W., Dalgarno, D., and Zhu, X. (2007). Crystal structure of the T315I mutant of AbI kinase. Chem Biol Drug Des *70*, 171-181.